SOFT ROBOTICS
Volume 00, Number 00, 2020

DOI: 10.1089/soro.2019.0156

SoRo
Soft Robotics

# Flexoskeleton Printing Enables Versatile Fabrication of Hybrid Soft and Rigid Robots

Mingsong Jiang, Ziyi Zhou, and Nicholas Gravish



## Abstract

One of the many secrets to the success and prevalence of insects is their versatile, robust, and complex exoskeleton morphology. A fundamental challenge in insect-inspired robotics has been the fabrication of robotic exoskeletons that can match the complexity of exoskeleton structural mechanics. Hybrid robots composed of rigid and soft elements have previously required access to expensive multi-material three-dimensional (3D) printers, multistep casting and machining processes, or limited material choice when using consumer-grade fabrication methods. In this study, we introduce a new design and fabrication process to rapidly construct flexible exoskeleton-inspired robots called ''flexoskeleton printing.'' We modify a consumer-grade fused deposition modeling (FDM) 3D printer to deposit filament directly onto a heated thermoplastic base layer, which provides extremely strong bond strength between deposited material and the inextensible, flexible base layer. This process significantly improves the fatigue resistance of printed components and enables a new class of insect-inspired robot morphologies. We demonstrate these capabilities through design and testing of a wide library of canonical flexoskeleton elements; ultimately leading to the integration of elements into a flexoskeleton walking legged robot.

**Keywords:** exoskeleton, flexoskeleton printing, rapid prototyping, programmable stiffness, continuum robotic leg, insect-inspired robots

## Introduction

The huge diversity of body morphologies and locomotion capabilities in the insect world have long served as inspiration for the design and control of flying,[1,2] swimming,[3,4] and walking robots.[5–7] A defining feature of insects (and more broadly all arthropods) is their external skeleton, called an exoskeleton, which must serve multiple roles including structural support, joint flexibility, joint and body protection, and providing functional surface features for sensing, grasping, and adhesion[8] (Fig. 1). The exoskeleton of all insects is a continuous sheath encompassing the animal, largely formed from two materials: chitin networks that are embedded within cuticular proteins.[9,10] Variation in exoskeleton stiffness (and other mechanical properties) occurs within the continuum of the exoskeleton to distinguish joints, struts, and continuously flexible regions (Fig. 1a). Both stiffness gradients, and discrete changes in stiffness, are controlled by variations in exoskeleton thickness, sclerotization, and geometry. Critically, the mobility and functional capabilities of insect limbs are determined by this arrangement of rigid, soft, and graded stiffness elements. The insect exoskeleton truly embodies a hybrid structure of rigid and soft mechanical elements.[9,11,12]

Animals, including insects, have long served as inspiration for robotics.[3,13–15] However, until recently, bioinspired robots tended to look like their rigid industrial robot counterparts, with legs and joints built from rigid links and stiff, high-gear ratio motors.[16,17] More recently, roboticists have begun adopting a bioinspired approach to robot structure, intentionally including body and limb compliance in robot designs.[15,18–21] New fabrication methods were developed to support this new direction in bioinspired robotics including shape-deposition manufacturing,[22–26] multi-material three-dimensional (3D) printing,[27,28] laser-cutting and lamination,[1,29–31] and mold-casting.[32,33] However, the use of these techniques has often relied on access to expensive and time-consuming fabrication tools with multistep processes and

Department of Mechanical and Aerospace Engineering, University of California, San Diego, La Jolla, California.

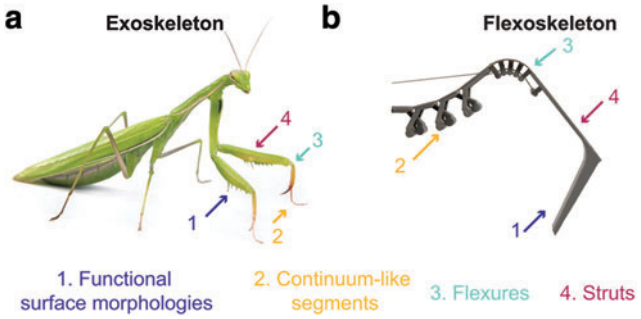


**FIG. 1.** **(a)** The exoskeleton of an insect provides protection and serves to support locomotion through structural and flexural regions. **(b)** In this article, we introduce a new method for fabricating exoskeleton-inspired robots that seek to embody the four principles of the exoskeleton. Color images are available online.

limited materials selection. One notable exception is origami and laminate-based robots, which can be fabricated using low-cost laser and paper cutters and assembled in a short time[34–36]; however, these planar methods do not allow the designer to directly design in three dimensions and require additional folding and bonding steps to complete fabrication.

In this article, we introduce a novel fabrication process called ''flexoskeleton'' printing to 3D print flexible and resilient robot exoskeletons for insect-inspired robots. This method uses low-cost fused deposition modeling (FDM) 3D printers and standard rigid filament materials acrylonitrile butadiene styrene/polylactic acid (ABS/PLA) that is readily accessible. The fundamental advance of our method relies on 3D printing rigid filaments directly onto a heated thermoplastic film, which provides a flexible, yet strong base layer to the deposited material. This fabrication method enables precise control of the arrangement and stiffness properties of joints and struts within the continuum structure of the robot body and its ease of use will enable wide adoption and significantly reduced fabrication times for bioinspired robotics.

Below we describe in detail the flexoskeleton fabrication process. We begin with a description of the fabrication process and experiments to demonstrate the robustness and fatigue resistance of these structures. We then present a library of flexoskeleton components that enable control of joint stiffness and bending limits. Integration of multiple joint elements into a single structure enables complex motion from multi-jointed legs that can be optimized for robot walking behavior. Finally, we demonstrate the capabilities of this rapid design and fabrication process by building and testing a quadruped flexoskeleton walking robot.

## Materials and Methods

### *Flexoskeleton printing*

The flexoskeleton printing process involves a simple modification to the standard FDM approach to 3D printing. In a standard consumer-grade FDM printer, a plastic filament such as ABS or PLA is extruded through the aperture of a heated nozzle and deposited onto a flat print surface. Many consumer FDM printers enable control of the print surface temperature as well, so that the printed material can resist warping from thermal gradients during the print process. In the flexoskeleton printing process, we adhere a thin sheet of polycarbonate (PC), a thermoplastic that can be softened and molded under heating, to the heated bed upon which we directly print. By heating the PC, we are able to achieve very strong adhesion between the 3D printed material and this base layer, which enables the printing of resilient flexible structures on standard consumer FDM printers.

In this study, we performed all our printing using either the Prusa i3 MK3S or the LulzBot Taz 6, two commercially available and consumer-grade FDM printers. We have demonstrated successful flexoskeleton printing with both ABS and PLA filament (HATCHBOX filament, diameter 1.75 mm) printed directly onto a thermoplastic backing film (PC, 0.1–0.2 mm). The print process begins by securing the base layer PC film on to the heated bed surface using a standard adhesive such as a washable glue stick (Fig. 2 and Supplementary Video S1). To further reduce warping of the PC, we additionally tape down the edges using high temperature masking tape. We next allow the bed temperature to reach the desired temperature, typically between 80°C and 100°C. To allow the first deposited layer to achieve close contact with the PC layer, and to create enough contact pressure for good bonding, we set a relatively small Z-offset between 0.01 and 0.03 mm above the film surface. The nozzle was heated up to 215°C for PLA and 240°C for ABS during the whole print. After the full print operation is finished, we first allow the heated bed and part to cool, which depending on the size of the part can be 5–10 min. Once the bed has cooled, we peel off the PC layer, including the bonded 3D printed components, and we remove the excess PC layer as the design dictates (Fig. 2a–c). We currently manually trim the PC layer with a cutting tool such as scissors or a razor; however, future flexoskeleton processes may integrate automated precutting of the PC film using a vinyl cutter or laser cutter (as applicable to the base layer material).

## Results

### *Delamination and fatigue resistance*

High bonding strength between the constitutive materials in either laminate fabrication[35,37] or multi-material 3D printing[38] is one of the most desirable mechanical properties to improve component lifespan and usability. For multilayered laminate robots, sheet adhesives (double-sided tape, thermoset adhesives) and liquid adhesives (epoxies, cyanoacrylate) have been extensively used for bonding.[39] While these adhesives are often extremely strong, application requires a multistep alignment and bonding process. Multi-material 3D printing also relies on the bonding strength between dissimilar materials that are printed into the continuum structure. High-end multi-material printers are often able to achieve strong bonding performance between rigid and soft materials; however, this comes at the expense of long print times, expensive print materials, and expensive printers. Alternatively, consumer-grade multi-material printing capabilities are emerging but suffer similar challenges in print time with relatively poor bond strength between dissimilar materials.[40,41]

The bonding process for flexoskeleton printing does not require additional adhesives or curing agents as the filament will be directly bonded to the base PC layer during extrusion. With a combined temperature and pressure, a process called, direct thermal bonding, between two thermoplastics take place where the flow of polymers at the material interface

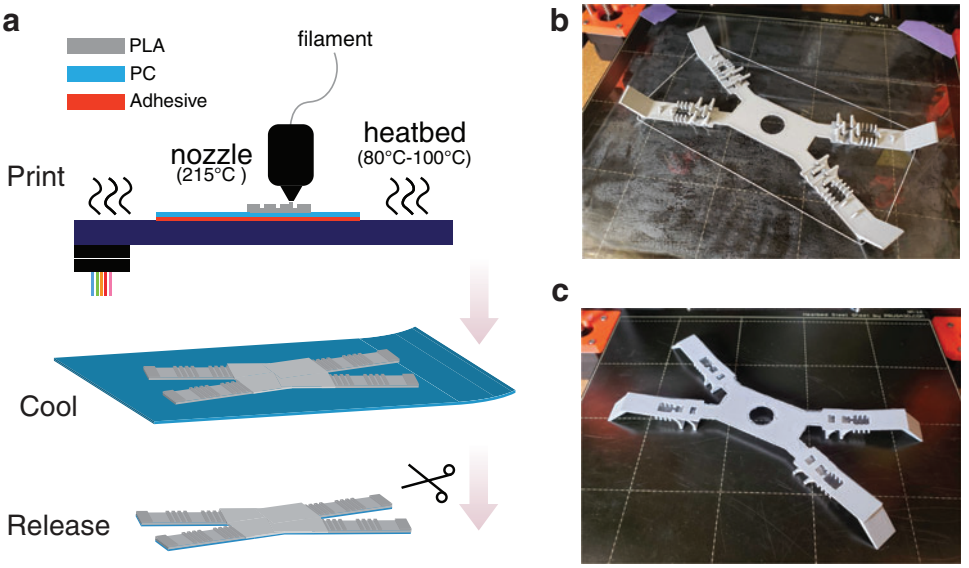


**FIG. 2.** Fabrication method. **(a)** Schematic of the flexoskeleton printing process. Printer filament polylactic acid or acrylonitrile butadiene styrene (PLA or ABS) is deposited on a heated layer of thermoplastic (PC). The PC is adhered to the surface of the print bed to remain flat during printing. Once printing is completed, the base layer and printed material are allowed to cool. After cooling, the part is released from the PC sheet by cutting. **(b)** An example of a four-legged robot immediately after printing on clear PC layer. **(c)** A four-legged robot after release from the PC layer. PC, polycarbonate. Color images are available online.

creates an entanglement of polymer chains leading to a strong bond between the two dissimilar materials.[42] The quality of the bond is thus likely to be sensitive to the bed temperature, while the nozzle temperature should be kept fixed to maintain print quality related to the filament (such as print resolution and stringing). To determine the optimal thermoplastic heating parameters for use on unmodified consumer FDM printers, we printed peel test samples with uniform geometry [40(L) × 12(W) × 2(T) mm] onto PC films (0.1 mm thickness) under varying heatbed temperatures (50–100°C). The peel test samples had a printed structure and a free PC tab. We conducted 180° peel tests by affixing the print structure in an Instron 3367 and pulling the tab around 180° attaching to the load cell of the Instron, we then peeled the PC layer from the printed sample (Fig. 3a, inset). The peel tests were conducted within a 6 mm peel range with a 3 mm/min peel speed. We measured the peel force during delamination and report the peel strength as a function of bed temperature. We find that for both ABS and PLA print material, the adhesion strength to PC is strongly dependent on heatbed temperature. Over the test ranges relevant to unmodified 3D printers, we observe a monotonically increasing bonding strength as we increase the heatbed temperature with 100°C providing the strongest adhesion (Fig. 3a). To give a tangible understanding of the high peel strength, we conducted a simple demonstration where a rectangular printed hook (surface area 12 × 34 mm) was able to pick up a 3.4 kg weight using a string without being delaminated (Fig. 3b). Furthermore, we also find that the peel strength can exceed that of commercially available high-bond acrylic sheet adhesives (3 M high bond transfer tape, 90° peel test, 11.2 N/cm onto ABS) demonstrating the strong delamination resistance of flexoskeleton components.

One critical challenge facing FDM 3D printed components that use standard filaments (ABS/PLA) is its low fatigue resistance.[43,44] Consumer-grade printed components typically will quickly yield or break under cyclic loading conditions, and thus are not recommended for using as long-term bending flexures especially with large bending range.[45,46] Flexoskeleton printed components on the other hand may overcome rapid fatigue and failure as the PC base layer acts as a tension-resistive protective layer. Compared with ABS and PLA filament, PC film has high flexural resilience, good impact resistance and toughness, and high tensile strength. Thus, the addition of a PC layer may reduce the amount of plastic deformation and fatigue that shallow layers of FDM printed components typically experience.

To test this hypothesis, we fabricated flexible beams with uniform rectangular geometries [48(L) × 22(W) × 0.4(T) mm] under three conditions: a standard printed control sample with no PC layer and two flexoskeleton beams with PC layers of 0.1 and 0.2 mm. We mounted the samples on a cyclic loading apparatus that bent the beams unidirectionally between a rest position and desired bend condition. In this test, we bent each beam to a constant stress state and maintained this position for 10 s to simulate scenarios where robot legs will be bent and held in place for load support. The load is then applied a distance 32 mm away from the rotary center using a rigid beam. We attempted to keep the maximum bending stress approximately the same by adjusting the maximum bending amplitudes among all samples so that the maximum bending torque was constant. We assume that the Young's modulus for PC and the print filament was comparable, and we kept the cross-sectional area the same across all different testing samples. We measured the creep angle of the beam by taking an image of the unloaded beam deflection angle as measured from the neutral position before testing. We find that by adding a PC layer we are able to reduce the creep deformation of 3D printed beams by 70% over a 300 load cycle period (Fig. 3c). The thickness of the PC layer for the two samples did not further contribute to the creep behavior of these beams during cyclic bending moments. Further experiments were performed to determine the fatigue resistance over large bending angle. We constructed flexures with and without PC backing using the same geometries as the creep experiment (five replicates each); the beams were bent to an angle of 60° at a constant rate of 1 Hz over 10,000 cycles. We recorded the neutral angle of the beams with a camera and determined when the beams failed, which was clearly identified as a sharp change in the neutral angle by breaking at the base. These long-term fatigue tests show

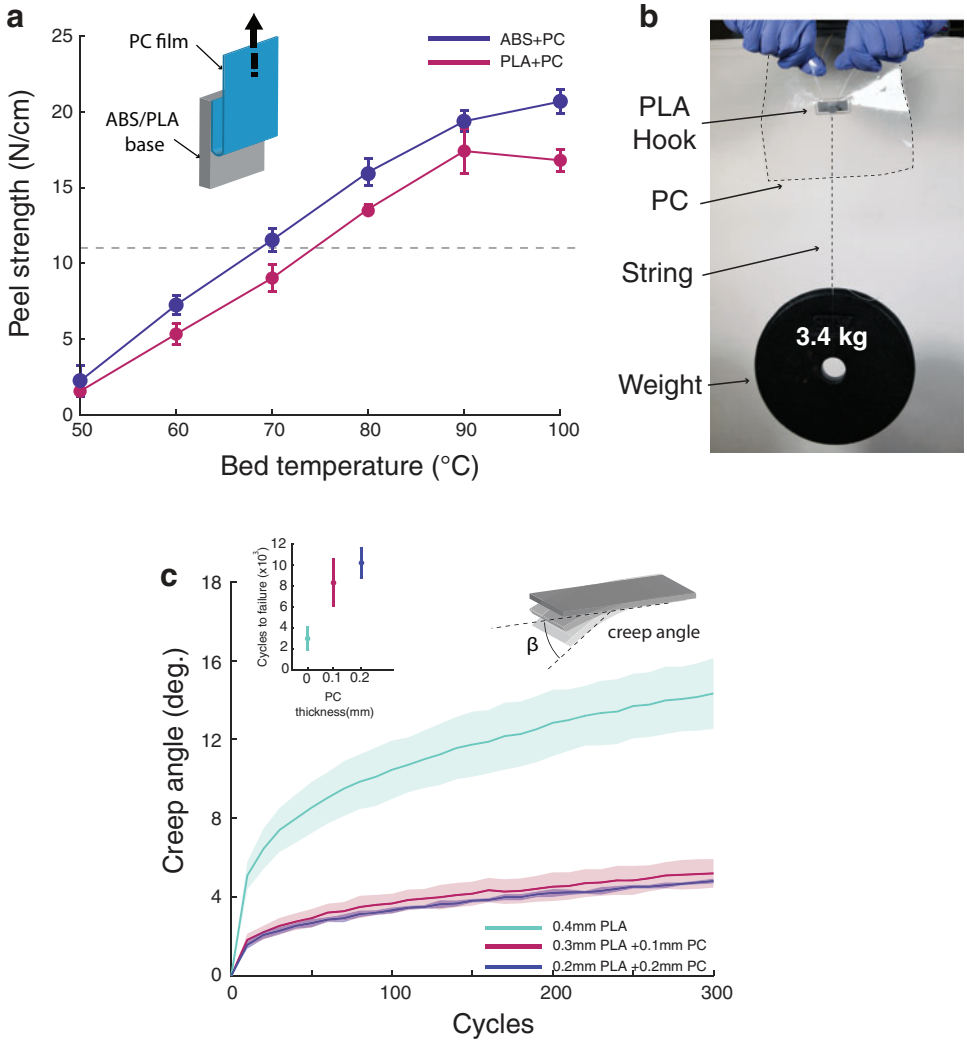


**FIG. 3.** Examples of resistance to delamination and fatigue. **(a)** The bed temperature determines the delamination peel strength between the PC layer and the 3D printed features. Peel strength in 180° peel tests increased to a maximum at 90–100°C. The *dashed line* indicates the peel strength (90° peel test) between a standard industrial acrylic adhesive on ABS for reference. **(b)** Proper print settings enable strong resistance to delamination between 3D printed features and the PC layer. Here, a 12×34 mm rectangle printed onto the PC layer is able to hold up a 3.4 kg weight. **(c)** Cyclic bend tests of constant thickness flexures printed with (*red* and *blue*) and without (*green*) show significantly less creep over time. Inset shows cycles to failure under 60° bend angle. Color images are available online.



similar results as creep tests in which the PC layer to an ~4× greater fatigue resistance (inset in Fig. 3c). These experiments demonstrate how the flexoskeleton printing process can enable direct printing of flexures and structures into a single continuum for bioinspired robotic exoskeletons.

### *A library of programmable stiffness subcomponents*

Having demonstrated the viability of flexoskeleton printing for creating resilient flexure elements, we now explore how the morphological features of the printed layer can be modulated to control bending properties. First, we investigate how flexural stiffness can be controlled by printing simple linear patterns. One way to modulate the bending stiffness of the flexure is by increasing the printing thickness of the deposited materials. However, as most consumer-grade printers can only print layers at a poor resolution (~0.1–0.3 mm layer resolution), depositing uniform layers may not enable fine-scale control of bending stiffness. Instead, a simple design principle for stiffness control is demonstrated in which linear patterns of high and low segments are printed across the flexure region (Fig. 4a). Here, the thickness of the segment is defined as ''feature height'' and the ratio of the raised feature's width versus period is defined as the ''feature width ratio.'' We then controlled these two design parameters separately and performed linear stiffness tests by using a custom-built rotary testing stage and measuring stiffness under small bending angle.

The measurement of the linear flexure stiffness was based on a custom motorized stage and force sensor setup. We mounted a load cell (LSB 200; Futek) on a rotary disk stage, which applied normal force directly onto the free end of the flexure. The free end was loaded along a circular path while force was measured. The test samples are 30(L)×44(W) mm with a base thickness of 0.3 mm (0.1 mm PC film +0.2 mm base PLA). Two parameters of the test samples varied: feature height ranging from 0.2 to 2 mm and feature width ranging from 0 to 4 mm (0–80%) within a 5 mm feature cycle (one repeatable line segment). The samples were mounted with their base fixed at the center axis of the rotary stage. The test is then begun by driving the stage at 0.5°/s in a 4° bending range with the segmented pattern on the flexure facing toward the load cell. The linear stiffness is then calculated as the force applied divided by the circular path travelled (N/m).

As shown in Figure 4a, changing the feature height results in relatively poor control of joint stiffness since the stiffness curve eventually reaches a plateau as height increases. However, changing the feature width ratio provides an effective method for control of flexure bending stiffness (Fig. 4b). The

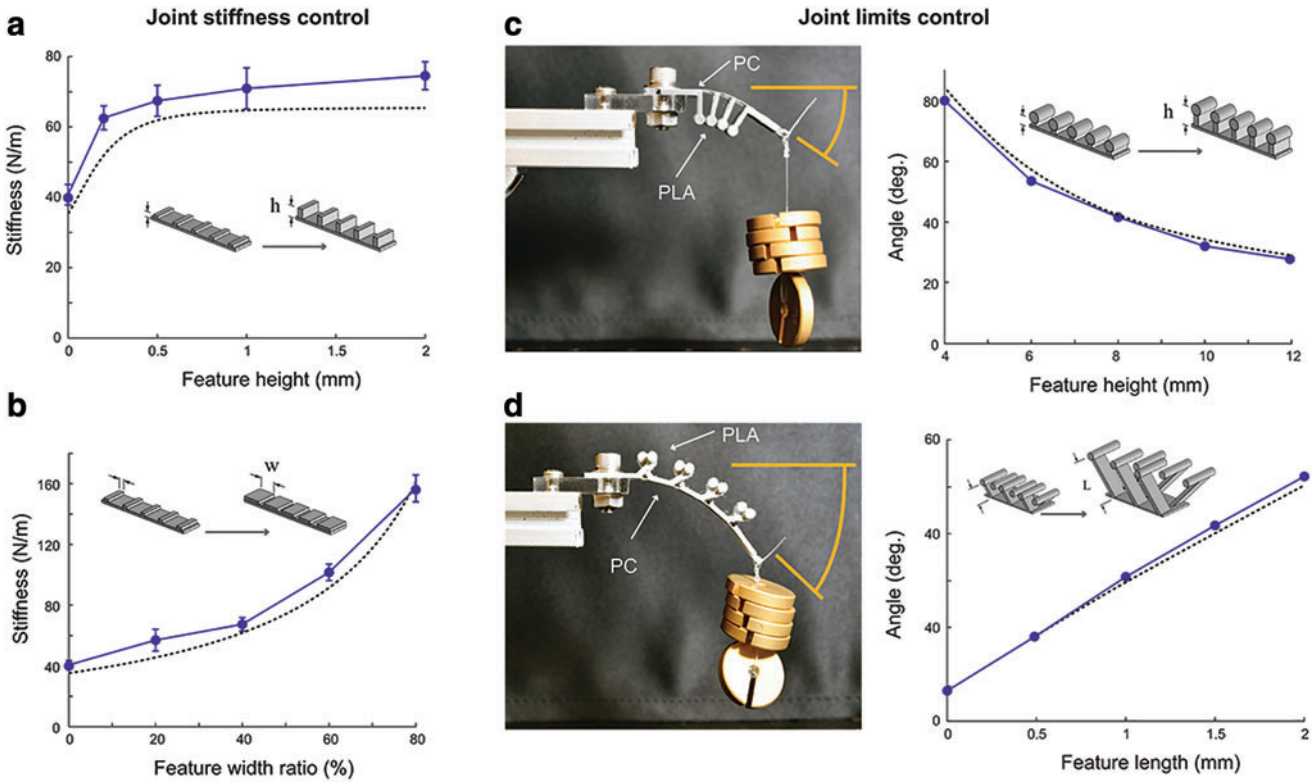


**FIG. 4.** Flexoskeleton design features. **(a, b)** Control of flexure mechanical stiffness is controlled by the width and height of rib features printed on the flexure. **(c, d)** To limit the angular range of printed flexure joints, we design jamming features that stop joint motion at a desired angle. Joint limits can be introduced in both the flexion **(c)** and extension **(d)** directions. *Dashed lines* represent theoretical model predictions (see Supplementary Data Modeling Derivation). Color images are available online.

predicted stiffness for all samples (dashed line) is based on a simple Euler Bernoulli beam theory model that only uses geometric and material parameters (Supplementary Data). Control of joint and flexure mechanical properties through geometry is a defining feature of flexoskeleton components since only a single print material is used. The ability to finely print repeated patterns enables good control over joint mechanical properties.

In addition to control of joint stiffness, many animals and robots possess joint stops to limit a joint's range of motion. Here, we demonstrate two types of flexoskeleton joint limits, which are both based on the principle of jamming between extruded features at a desired bend angle. Flexional joint limits are composed of vertical pillars with a circular end that serve to jam together and significantly stiffen the joint (Fig. 4c). The distance between the center of the head to the base layer is defined as the ''feature height,'' and a simple geometrical model (Supplementary Data) dependent on these parameters is provided. Here, we report programmable joint limits by varying the feature height (Fig. 4c, right). By reversing the order of the adjacent jammable features for every two stand outs, we reversed the direction in which the jamming happens and thus created extensional joint limits stiffening the joint at large extensions of the joint. Here, we defined the feature length as the diagonal length of the geometrical standouts and measured jamming angles versus this control parameter. In all instances, we find good agreement between measurements of the jamming angle and a simple geometrical model of flexure bending (Supplementary Data).

### *Complex limb motions determined by leg mechanical properties*

As explored in the previous section, adding geometric features to the printed layers can enable a wide variety of flexure bending mechanical properties, such as variable bending stiffness, and joint limits. These features can thus be integrated into a robotic limb for programmable limb motions. As a demonstration of generating complex motions in underactuated flexoskeleton limbs, we designed a flexoskeleton leg composed of two flexural joints: a flexion joint for limb contraction and an extension joint for lifting the foot tip. For each joint, we prescribed the passive joint stiffness (determined by the segmented patterns) and joint limits (flexion and extension) and used a single tendon to actuate the two joints by routing it above the extension joint and below the flexion joint (Fig. 5a). We present the design of the hind limb as an example, to achieve a nonrepeatable limb cycle, we printed higher passive joint stiffness for the flexion joint but lower passive joint stiffness for the extension joint. This enables the leg to lift first then contract back and downward for a foot displacement without touching the ground (Fig. 5b). As the tendon releases, asymmetric friction at the toe and tendon cause the foot to generate a push motion against the ground and thus enabling hysteretic foot motion via a single tendon. The total displacement of the push stroke is controlled by the jamming hinge angles and stiffnesses. As an exploration of this, we changed the design of the extensional joint limits, observing different foot trajectories (Fig. 5c) and

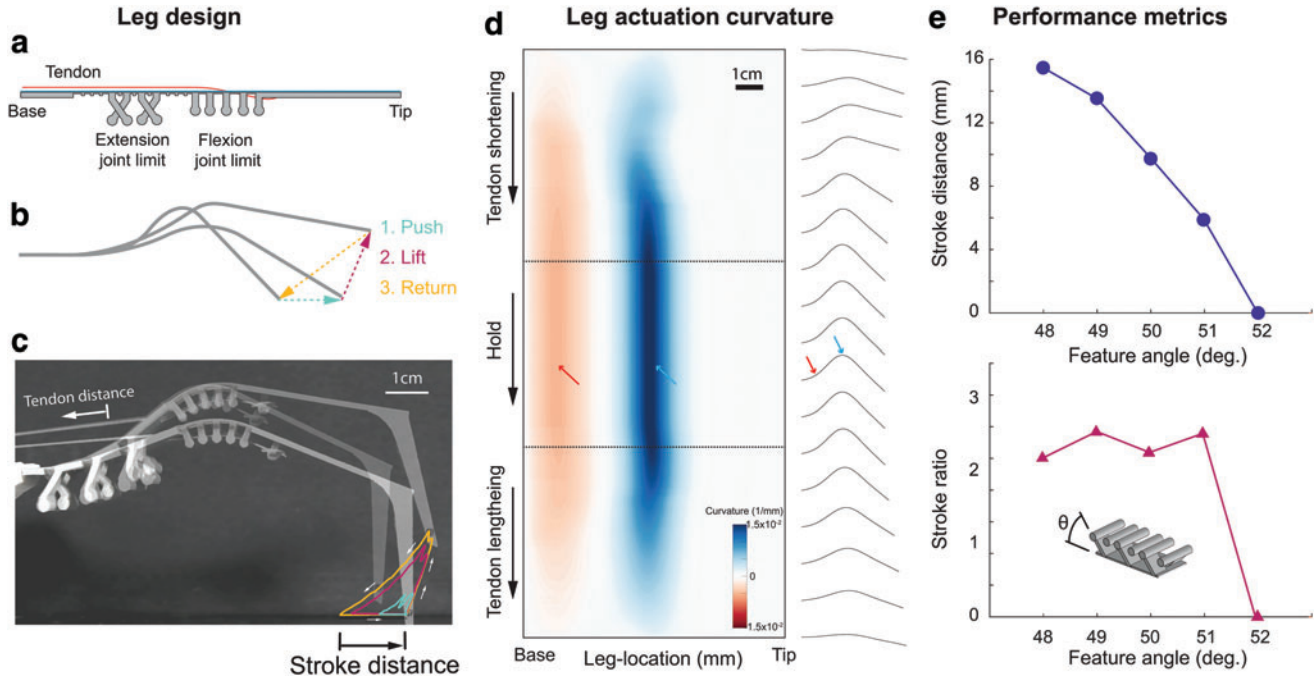


**FIG. 5.** Limb motion control through mechanically programmable joint properties. **(a)** Design of one robotic limb, composed of both extension joint and flexion joint with programmable linear stiffness and joint limits. **(b)** The motion sequence of a hind leg from pulling and releasing of one tendon. **(c)** Foot trajectories tracked from within one limb motion cycle with different jamming feature angles (*yellow*: 48°, *red*: 49°, and *green*: 51°). **(d)** Heat map of the leg actuation curvature (*right*) and the shape of the continuum limb outlier (*left*) changing as a function of the tendon state. **(e)** Stroke distance (*top*) and stroke ratio (*bottom*), defined as stroke distance per unit tendon pull distance as measured from different feature angles (from 48° to 52°). Color images are available online.

measuring the limb curvature and shape change (Fig. 5d) and stroke properties (Fig. 5e). Tracking the continuous curvature of the limb during the actuation cycle highlights how flexoskeleton limbs behave as a continuum structure with a gradient in shape and curvature (Fig. 5d). This is in stark contrast to more traditional link-joint limb designs in which the curvature would be observed as a delta function at each joint.

The stroke distance as well as the stroke ratio (defined as stroke distance per unit tendon pull distance) is controlled by the properties of the limb hinges, and in Figure 5e, we highlight how changing the jamming angle of the extensional hinge alone can change the limb stroke. We find that by having different designs of the jamming morphology, one can achieve different stroke distances without large changes of the stroke ratio, whereas changing the programmable passive joint stiffness allows for different walk sequences and thus the functionality of the limb. The design of the front limbs can be achieved by having the opposite stiffness distribution as in the hind limb, which enables a pull-lift cycle of movement.

### *Walking performance of a flexoskeleton walking robot*

As a demonstration of the walking capabilities of a rapidly prototyped flexoskeleton robot, we built a tendon-driven four-legged flexoskeleton walking robot. The robot is designed and assembled using all flexoskeleton printed limbs and chassis and is actuated by four micro servos (Fig. 6a, Tower Pro SG92R). The legs consist of a 70 mm length flexoskeleton continuum limb with two joints: one flexion and one extension. We designed flexional limit that can be jammed at 90°, with a total joint length of 10 mm and extensional limit jamming at 20° with a total joint length of 22 mm. We chose the front limbs and hind limbs to have similar bending stiffness properties; however, the high and low stiffness of the flexional and extensional joints were reversed between hind and front limbs to reverse the stroke direction. For the hind limb design, we made the extension joint (0.2 mm PC +0.3 mm PLA) a bit stiffer than the flexional joint (0.2 mm PC +0.1 mm PLA), whereas in the front limb design, the case was reversed. Such a design can help the hind limb to generate a lift-push gait cycle with the front limb doing a pull-lift gait cycle. Each limb is printed within 30 min with the total print time for the whole robot around 3 h using one 3D printer. The layer height is set as 0.2 mm with an infill of 30% for the robot chassis.

Each limb is then inserted into the robot chassis (body) and connected with one micro servo through a single tendon and a capstan. We designed the legs to be modular such that limb designs are able to be rapidly swapped out on the robot to suit different gait requirements or walking terrains (such as smooth or rough substrates). Note that the robot can also be printed within one print if certain joint parameters are preprogrammed to meet with specific walking requirements. For robot operation, we first started the robot by applying pretension in the tendon to support the whole body weight (78 g) while standing (Fig. 6a). The joint limits can further help the robot support the stationary body weight by stiffening the joint at the extreme flexion or extension angles. We then programmed a biped walking gait with two diagonal pairs (e.g., front left and hind right as one pair) walking out of

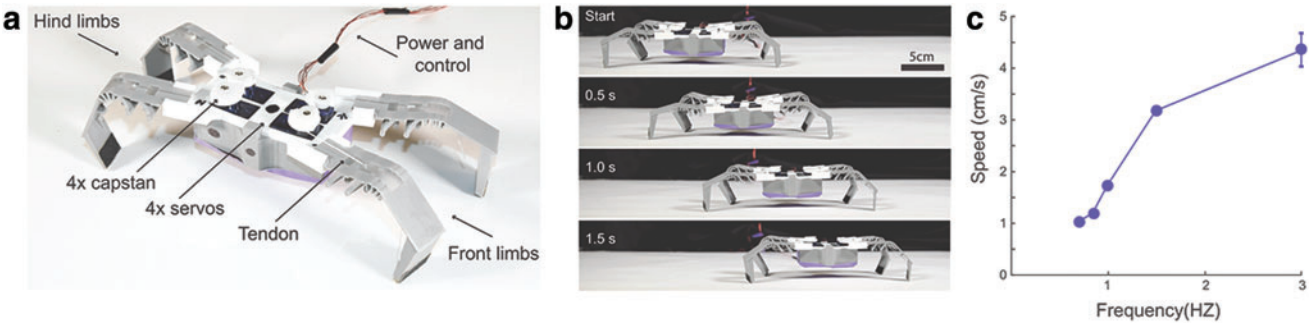


**FIG. 6.** A walking quadruped flexoskeleton robot. **(a)** Each limb is actuated by a single servo and tendon. Off-board power and control are provided through a tether. **(b)** A side view of a walking sequence. **(c)** Speed–frequency relationship of the walking performance of the robot. Color images are available online.



phase with the same frequency (Fig. 6b and Supplementary Video S2). The walking speed was recorded under different driving frequencies on a flat surface with paper substrate, and the speeds were measured and averaged over a 0.8 m walking distance using a camera for observation (Fig. 6c).

### *Opportunities and challenges for hybrid stiffness flexoskeleton robots*

The flexoskeleton printing process provides a versatile and easily accessible fabrication method for rapid prototyping of flexible, continuum, and hybrid rigid–soft robots and fits well within the other suite of tools for creating soft robots (Supplementary Table S1 and Supplementary Data). Flexoskeleton fabrication enables an alternative design process to that of typical 3D printing. When a roboticist or designer works with a standard 3D printing process, they typically begin with a rigid structure as the starting point (since most print materials are rigid) and then intentionally include flexibility through geometry or print material gradations. With the flexoskeleton process, we argue that the design methodology is the opposite; the PC backing provides an initial inherently flexible substrate upon which rigid material is intentionally deposited.

An additional benefit that flexoskeleton printing provides is minimization of manual assembly steps for creating articulated 3D printed components. Fabrication of a rigid link-joint based robot using a 3D printer would typically require printing each link separately and then hand aligning and assembling the components. In a flexoskeleton robot the joint geometry is precisely defined by the printer and so the precision of articulated components can be increased using this process. Flexoskeleton printing can even be used for simplifying the printing of fully rigid designs, much like flexures in an origami robot can enable the precise locating of folds that will eventually be locked in place,[29,35] a similar concept can be used in flexoskeleton designs where flexible PC regions can be used to locate precision assembly of components.

Flexoskeleton printing can also improve the longevity of 3D printed living hinges. Our experiments demonstrate that the addition of a flexible PC backing layer improves creep resistance and time to failure for flexible joints. However, there is still significant improvements to be made in terms of fatigue resistance for flexoskeleton printing as the time to failure of bending hinges is still quite low for any practical purposes beyond prototyping. Flexoskeleton printing provides an incredibly quick method for reliably making flexible robotic components, which will greatly speed up design and prototyping iterations. However, due to the rapid fatigue and low strength of common 3D printing plastics, substantial improvements will be required if this process is to be implemented for production ready robots.

The mechanical properties of the PC backing layer place limitations on the types of structures and shapes that can be created through flexoskeleton printing. For example, the PC layer is stiff and can be assumed to be inextensible, which limits the ways in which flexoskeleton structures can bend. Inextensible sheets can only curve along a single axis and thus cannot be bent into nondevelopable shapes (such as a spherical shells). Cutting reliefs in the PC may enable more complicated benign patterns; however, this requires foreknowledge of the exact bends the flexoskeleton will undergo. There are many future opportunities for incorporating different, extensible, and stretchy backing layers, such as elastomeric PC sheets.

## Conclusion

The insect exoskeleton serves both as a protective exterior and as a mechanical transmission that routes power from muscles to limbs. The exoskeleton is a multi-material continuum in which rigid and soft tissues are organized in complex 3D arrangements. Critically, the arrangement of these rigid and soft regions form functional mechanical systems such as linkages,[47] springs,[48,49] and even gears.[50] Robot morphologies inspired by the insect exoskeleton may enable new multifunctional robots and further help us understand how complex arrangements of compliant elements can enable power transmission and control of biological locomotion.

Inspired by the insect exoskeleton, in the work described here, we present a new fabrication process called ''flexoskeleton'' printing that enables rapid and accessible fabrication of hybrid rigid–soft robots. Critically, this fabrication approach is extremely accessible to both novice and expert users and does not require exorbitant material or equipment costs. The approach we have developed relies heavily on the interrelationships between 3D geometry of surface features and their contributions to the local mechanical properties of that component. We envision that this method will enable a new class of bioinspired robots with focus on the interrelationships between mechanical design and locomotion.

### Authors' Contributions

N.G. and M.J. contributed to the conceptualization, design, and experiments in this work. M.J. and Z.Z. contributed to mechanical characterization and robot design and fabrication work. All authors contributed to writing.

### Acknowledgments

We thank the members of the Gravish Lab including Wei Zhou, Shivam Chopra, and Glenna Clifton for their helpful project comments.

### Author Disclosure Statement

No competing financial interests exist.

### Funding Information

Funding support was provided through the Department of Mechanical and Aerospace Engineering at the University of California, San Diego. Partial funding support was provided through NSF #1935324.

### Supplementary Material

Supplementary Data
Supplementary Figure S1
Supplementary Figure S2
Supplementary Table S1
Supplementary Video S1
Supplementary Video S2

### References

1. Ma KY, Chirarattananon P, Fuller SB, *et al.* Controlled flight of a biologically inspired, insect-scale robot. Science 2013;340:603–607.
2. Karásek M, Muijres FT, De Wagter C, *et al.* A tailless aerial robotic flapper reveals that flies use torque coupling in rapid banked turns. Science 2018;361:1089–1094.
3. Chen Y, Wang H, Farrell Helbling E, *et al.* A biologically inspired, flapping-wing, hybrid aerial-aquatic microrobot. Sci Robot 2017;2:eaao5619.
4. Ozcan O, Wang H, Taylor JD, *et al.* STRIDE II: a water strider-inspired miniature robot with circular footpads. Int J Adv Rob Syst 2014;11:85.
5. Saranli U, Buehler M, Koditschek DE. RHex: a simple and highly mobile hexapod robot. Int J Rob Res 2001;20:616–631.
6. Birkmeyer P, Peterson K, Fearing RS. DASH: A dynamic 16g hexapedal robot. In 2009 IEEE/RSJ International Conference on Intelligent Robots and Systems. St. Louis, MO: 2009, pp. 2683–2689.
7. Kim S, Clark JE, Cutkosky MR. iSprawl: design and tuning for high-speed autonomous open-loop running. Int J Rob Res 2006;25:903–912.
8. Nishino H, Domae M, Takanashi T, *et al.* Cricket tympanal organ revisited: morphology, development and possible functions of the adult-specific chitin core beneath the anterior tympanal membrane. Cell Tissue Res 2019;377:193–214.
9. Klowden MJ. Physiological Systems in Insects. London: Academic Press, 2013.
10. Clark AJ, Triblehorn JD. Mechanical properties of the cuticles of three cockroach species that differ in their wind-evoked escape behavior. PeerJ 2014;2e501.
11. Kovač M. The bioinspiration design paradigm: a perspective for soft robotics. Soft Robot 2013;1:28–37.
12. Jayaram K, Full RJ. Cockroaches traverse crevices, crawl rapidly in confined spaces, and inspire a soft, legged robot. Proc Natl Acad Sci U S A 2016;113:E950–E957.
13. Koh J-S, Yang E, Jung G-P, *et al.* Biomechanics. Jumping on water: surface tension-dominated jumping of water striders and robotic insects. Science 2015;349:517–521.
14. Jafferis NT, Helbling EF, Karpelson M, *et al.* Untethered flight of an insect-sized flapping-wing microscale aerial vehicle. Nature 2019;570:491–495.
15. Umedachi T, Vikas V, Trimmer BA. Softworms: the design and control of non-pneumatic, 3D-printed, deformable robots. Bioinspir Biomim 2016;11:025001.
16. Raibert MH. Legged robots. Commun ACM 1986;29:499–514.
17. Todd DJ. Walking Machines: An Introduction to Legged Robots. London: Springer Science & Business Media, 2013.
18. Kim S, Laschi C, Trimmer B. Soft robotics: a bioinspired evolution in robotics. Trends Biotechnol 2013;31:287–294.
19. Blickhan R, Seyfarth A, Geyer H, *et al.* Intelligence by mechanics. Philos Trans A Math Phys Eng Sci 2007;365:199–220.
20. Paul C. Morphological computation: a basis for the analysis of morphology and control requirements. Rob Auton Syst 2006;54:619–630.
21. Pfeifer R, Iida F, Lungarella M. Cognition from the bottom up: on biological inspiration, body morphology, and soft materials. Trends Cogn Sci 2014;18:404–413.
22. Cham JG, Bailey SA, Clark JE, *et al.* Fast and robust: hexapedal robots via shape deposition manufacturing. Int J Rob Res 2002;21:869–882.
23. Bailey SA, Cham JG, Cutkosky MR, *et al.* Biomimetic robotic mechanisms via shape deposition manufacturing. In: Hollerbach JM, Koditschek DE (Eds). Robotics Research. London: Springer, 2000, pp. 403–410.
24. Gul JZ, Sajid M, Rehman MM, *et al.* 3D printing for soft robotics—a review. Sci Technol Adv Mater 2018;19:243–262.
25. Wallin TJ, Pikul J, Shepherd RF. 3D printing of soft robotic systems. Nat Rev Mater 2018;3:84–100.
26. Yirmibesoglu OD, Morrow J, Walker S, *et al.* Direct 3D printing of silicone elastomer soft robots and their performance comparison with molded counterparts. In 2018 IEEE International Conference on Soft Robotics (RoboSoft), 2018, pp. 295–302.
27. Bartlett NW, Tolley MT, Overvelde JTB, *et al.* A 3D-printed, functionally graded soft robot powered by combustion. Science 2015;349:161–165.
28. Schaffner M, Faber JA, Pianegonda L, *et al.* 3D printing of robotic soft actuators with programmable bioinspired architectures. Nat Commun 2018;9:878.
29. Wood RJ, Avadhanula S, Sahai R, *et al.* Microrobot design using fiber reinforced composites. J Mech Des 2008;130:052304.
30. Baisch AT, Heimlich C, Karpelson M, *et al.* HAMR3: an autonomous 1.7g ambulatory robot. In 2011 IEEE/RSJ International Conference on Intelligent Robots and Systems. San Francisco, CA: 2011, pp. 5073–5079.
31. Felton S, Tolley M, Demaine E, *et al.* A method for building self-folding machines. Science 2014;345:644–646.
32. Seok S, Onal CD, Cho K-J, *et al.* Meshworm: a peristaltic soft robot with antagonistic nickel titanium coil actuators. IEEE/ASME Trans Mechatron 2013;18:1485–1497.

33. Holland DP, Park EJ, Polygerinos P, *et al.* The Soft Robotics Toolkit: shared resources for research and design. Soft Robot 2014;1:224–230.
34. Sung C, Rus D. Foldable joints for foldable robots. J Mech Robot 2015;7:021012-1–021012-13.
35. Haldane DW, Casarez CS, Karras JT, *et al.* Integrated manufacture of exoskeletons and sensing structures for folded millirobots. J Mech Robot 2015;7:021011.
36. Onal CD, Tolley MT, Wood RJ, *et al.* Origami-inspired printed robots. IEEE/ASME Trans Mechatron 2015;20: 2214–2221.
37. Correa JE, Toombs J, Toombs N, *et al.* Laminated micromachine: design and fabrication of a flexure-based delta robot. J Manuf Process 2016;24:370–375.
38. Wang X, Jiang M, Zhou Z, *et al.* 3D printing of polymer matrix composites: a review and prospective. Compos B 2017;110:442–458.
39. Cho K-J, Koh J-S, Kim S, *et al.* Review of manufacturing processes for soft biomimetic robots. Int J Precis Eng Manuf 2009;10:171–181.
40. Lumpe TS, Mueller J, Shea K. Tensile properties of multimaterial interfaces in 3D printed parts. Mater Des 2019; 162:1–9.
41. Belter JT, Dollar AM. Strengthening of 3D printed fused deposition manufactured parts using the fill compositing technique. PLoS One 2015;10:e0122915.
42. Yu S, Ng SP, Wang Z, *et al.* Thermal bonding of thermoplastic elastomer film to PMMA for microfluidic applications. Elsevier Enhanced Reader. https://www.sciencedirect.com/science/article/pii/S0257897216312786/pdfft?isDTMRedir=true&download=true (accessed July 29, 2019).
43. Letcher T, Waytashek M. Material property testing of 3D-printed specimen in PLA on an entry-level 3D printer. In ASME 2014 International Mechanical Engineering Congress and Exposition; American Society of Mechanical Engineers. Montreal: 2014, pp. V02AT02A014–V02AT02A014.
44. Ezeh OH, Susmel L. On the fatigue strength of 3D-printed polylactide (PLA). Procedia Struct Integrity 2018;9:29–36.
45. Song Y, Li Y, Song W, *et al.* Measurements of the mechanical response of unidirectional 3D-printed PLA. Mater Des 2017;123:154–164.
46. Kim H, Park E, Kim S, *et al.* Experimental study on mechanical properties of single- and dual-material 3D printed products. Procedia Manuf 2017;10:887–897.
47. Dallmann CJ, Dürr V, Schmitz J. Joint torques in a freely walking insect reveal distinct functions of leg joints in propulsion and posture control. Proc Biol Sci 2016;283:pii: 20151708.
48. Dickinson MH, Lighton JR. Muscle efficiency and elastic storage in the flight motor of drosophila. Science 1995;268: 87–90.
49. Vincent JFV, Wegst UGK. Design and mechanical properties of insect cuticle. Arthropod Struct Dev 2004;33:187–199.
50. Burrows M, Sutton G. Interacting gears synchronize propulsive leg movements in a jumping insect. Science 2013; 341:1254–1256.

Address correspondence to:
*Nicholas Gravish*
*Department of Mechanical and Aerospace Engineering*
*University of California, San Diego*
*La Jolla, CA*

*E-mail:* ngravish@eng.ucsd.edu